Applied Physics B (2023) 129:162
https://doi.org/10.1007/s00340-023-08096-7

Applied Physics B
Lasers and Optics

RESEARCH

A Hanbury Brown and Twiss renascence: measurement of photon correlations yields spatio-temporal coherence

Wolfgang Ruppel[1] · Peter Duerr[1] · Jan Ross[1] · Wolfgang Elsäßer[2,3,4]

Received: 17 July 2023 / Accepted: 28 August 2023 / Published online: 3 October 2023

Abstract
Investigations of photon correlations similar to the Hanbury Brown and Twiss experiment are since the advent of quantum optics in the center of both fundamental and application-oriented research. We derive a factorial moment-generating function of the probability distribution of electromagnetic radiation emitted by a source and absorbed by a photodetector from which we calculate an analytical expression for the second-order correlation coefficient $g^{(2)}$ which reflects spatial coherence properties of the emitted light. The measurement of $g^{(2)}$ thus allows to retrieve the spatial coherence parameter of the light source in terms of the combination of source area, source-detector distance, wavelength and detector area. The validity of the concept is proven by investigating $g^{(2)}$ of true thermal light from a Xenon arc lamp and from the sun for various detector areas, in excellent agreement with the theory. Finally, we suggest a novel scheme for determining light source diameters by exploiting the spatially dependent statistics and confirm its validity by exemplary calculations. These results based on radiation thermodynamics and photon statistics give fresh insight into quantum optical properties of classical light sources, photon correlations and photodetection with promising applications perspectives, more than 68 years after the original Hanbury Brown and Twiss experiment.

1 Introduction

The existing theory of photodetection goes back to Glauber [1], where he formulated in this pioneering work the quantum theory of photodetection and optical coherence. This theory is central to quantum optics and has played a key role in understanding light-matter interactions [2, 3]. This work has been followed by Mandel's semiclassical counting formula [4] relating the photo-clicks of the detector via a so-called Poisson Transform to the probability distribution of the impinging absorbed field or the intensity statistics [5]. However, even before this advent of quantum optics the Hanbury Brown and Twiss (HBT) experiment [6], now 67 years ago, set the foundation of nowadays understanding of light statistics in terms of correlations [7, 8]. The fundamental observation of photon bunching of a thermal light source, as also acknowledged in the Nobel award lecture of Glauber [9] led to the classification of light in terms of its second-order or intensity correlation coefficient. HBT had been astronomers from their profession driven by the search for improving stellar interferometry for determining the star diameter [10]. After the lab experiment with the observation of photon bunching of a thermal light source they returned back to the stellar interferometer in applying this newly proven and realized intensity interferometer to this original task [11]. The success story was huge and finds even today a perpetual continuation with new detector approaches and signal processing technologies investigating photon bunching [12, 13] and resulting already in a sort of HBT revival in astronomy [14–17] and with new aspects of light correlations [18, 19]. The original HBT intensity interferometer always exploits two intensity-detectors with the baseline separation L in

Peter Duerr and Jan Ross have contributed equally to this work.

W. Ruppel: deceased.

✉ Wolfgang Elsäßer
elsaesser@physik.tu-darmstadt.de

[1] Institute of Applied Physics, Karlsruhe Institute of Technology, Wolfgang-Gaede-Strasse 1, 76128 Karlsruhe, Germany

[2] Institute of Applied Physics, Technische Universität Darmstadt, Schlossgartenstrasse 7, 64289 Darmstadt, Germany

[3] School of Physics, Trinity College Dublin, Dublin 2, Ireland

[4] CNR-Istituto di Elettronica e di Ingegneria dell'Informazione e delle Telecomunicazioni (CNR-IEIIT), Corso Duca degli Abruzzi 24, 10129 Turin, Italy

between them for determining the second order intensity cross correlation $G^{(2)}(L) = \langle I_1(0)I_2(L)\rangle$ between the two intensities I_1 and I_2, respectively. From the characteristic decay of $G^{(2)}$ as a function of the baseline separation L finally the star diameter is derived. Our approach is a based on the autocorrelation determination $G^{(2)}(A) = \langle I(A)I(A)\rangle$ of the intensity I of a single detector as a function of the detector aperture A. Already in 1966, Martienssen and Spiller showed that the photon counting statistics of a so-called pseudo-thermal (PT) light source (laser light scattered at a rotating diffuser ([20, 21]) measured with a single photomultiplier shows a characteristic transition from Bose–Einstein statistics to Poisson statistics if either the separation between detector and source is decreased or, equivalently the diameter of the source is increased [22], thus revealing spatial coherence effects [23]. It has been also recognized that the measured statistics is effectively a Negative Binomial or Polya distribution [5] depending on the mode number N, being the effective mode number at the emitter surface or being $N = 1$ at infinity separation between source and detector, respectively. Bures et. al. [24, 25] performed comprehensive studies of the photon electron counting statistics of various types of this PT source, already using one single photon multiplier and analyzing the photon count statistics in terms of an ansatz for the moment-generating function and considering the degree of coherence of an extended light source in the framework of the Van-Zittert Zernike theorem [26, 27]. This $g^{(2)}$ approach has also been applied to investigations of scattered light [28].

At the beginning of quantum optics [29] measuring photon statistics has been a useful approach for understanding photon statistics of various light sources [23, 30–32], but even nowadays, $g^{(2)}$ measurement via HBT based correlation investigations or equivalently of the characteristic statistics of light is THE tool for the understanding of electromagnetic radiation [33] and the search and understanding of light emitters [18, 34–36], and even applicable to fermions [37] or photons in biological systems or photosynthesis [38–40]. Even super-bunched light with a $g^{(2)}$ value exceeding two had been achieved by doubly scattering of laser light [41–43]. Another very recent approach to generate new statistics focused on nonlinear optical processes [44, 45] or superbunching in twin photon generation [46–48]. These developments and the realization of novel photon source schemes have been accompanied by a comparable advancement in the detection and in the analysis of photon events [49–51]. This development demonstrates that today it is still a challenging field of research with impressive progress giving complete insight into the photon properties by novel detector signal analysis strategies and reconstruction techniques [52–55]. This research may incorporate inherent novel light sources or strategies to modify and tailor the light statistics according to the needs of applications, as e.g. in ghost modalities [56–58] as ghost imaging [59–61] or ghost spectroscopy [62] where tailored photon bunching directly determines the metrology advantages [63].

The aim of the present publication is to investigate the statistical properties of photo clicks or absorption events originating from the photon statistics. The method is traditional stochastic theory based on probability distributions and a factorial moment generating function finally being condensed in the second order intensity correlation coefficient. We start with a characteristic factorial moment generating functions consisting of a composite of a binomial function involving the photo-detection and a generalized Poisson distribution originating from the light source properties. We derive an analytical expression for the central second order correlation coefficient $g^{(2)}$ in terms of spatial and temporal coherence Z_s and Z_t, respectively [27]. Its dependencies are comprehensively discussed in terms of spatial coherence and thermodynamics of the source. Finally, we conceive and realize an experimental set-up which investigates $g^{(2)}$ of four different true thermal light source - detector configurations, a Xe arc lamp with three different detector dimensions and sun light. The good agreement between theory and experimental results verifies that this novel modified single-detector HBT concept allows to determine e.g. the source area if source distance is known, and this with a single-detector concept without any baseline separation, thus giving rise to a renascence of HBT.

2 Theoretical considerations

2.1 Schematical emission and detection scheme

The schematic of the emission and detection configuration for the basis of the calculations and the experiments is depicted in Fig. 1. Radiation with an emission wavelength λ is emitted by a light source with an emission area of A_{source} and is detected by an absorption process in a photodetector at a distance R and with detector area A_{detector} resulting in a number n of click events during a time interval Δt with a normalized probability distribution $P(n)$.

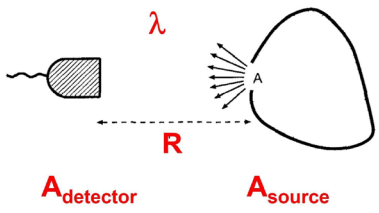

Fig. 1 Schematical depiction of the scheme for the investigations of the photon statistics with the source and the detector

We define the coherence parameter Z, which factorizes into the temporal coherence Z_t and the spatial coherence Z_s:

$$Z = Z_t \cdot Z_s = \Delta\nu\Delta t \cdot \frac{A_{\text{source}} A_{\text{detector}}}{\lambda^2 R^2} \tag{1}$$

Z_s may or may not again factorize into two parameters Z_x and Z_y in an obvious way, depending on the geometric shape of the light source and detector.

2.2 The factorial moment generating function

To calculate photon correlations we make use of the factorial moment-generating function (fmgf) $G(s)$, which is defined as

$$G(s) = \sum_{n=0}^{\infty} P(n)s^n \tag{2}$$

and together with the normalization of the probability distribution $\sum_{n=0}^{\infty} P(n) = 1$ leads to $G(s = 1) = 1$.

We start with a factorial moment-generating function $G(s)$ of the probability distribution of radiation absorbed by a photodetector yielding a distribution of clicks events as a consequence of the absorption events which has the type of a generalized binomial distribution. The derivation of this factorial moment-generating function $G(s)$ is performed in appendix C and D and we obtain

$$G(s) = \left(1 - n_{Ph}\eta p_Z(s-1)\right)^{\frac{-Z}{p_Z}} \tag{3}$$

with the average number of photons in a unit coherence volume n_{Ph}, the quantum efficiency of the detector η, and an a-priori probability p_Z which will be discussed below and in the appendix D.

2.3 Moment calculations and second order correlations coefficient for the fmgf

From the fmgf $G(s)$ (Eq. 2) we can directly obtain the factorial moments $\langle n(n-1)(n-2)...(n-1+k)\rangle$ according to [64]

$$\langle n(n-1)(n-2)...(n-1+k)\rangle = \frac{d^n}{ds^n} G(s)|s \to 1 \tag{4}$$

The second order correlation coefficient $g^{(2)}$ (We remind that throughout the manuscript $g^{(2)}$ means the central second order correlation coefficient $g^{(2)}(\tau = 0)$ for delay time $\tau = 0$ [64]) is defined as the ratio between the second order factorial moment $\langle n(n-1)\rangle$ and the square of the first order factorial moment $\langle n\rangle$ resulting finally in [64]

$$g^{(2)} = \frac{\langle n(n-1)\rangle}{(\langle n\rangle)^2} \tag{5}$$

For our fmgf in Eq. (3) we get:

$$g^{(2)} = \left(\frac{d^2}{ds^2} G(s)\big|_{s\to 1}\right) \Big/ \left(\frac{d}{ds} G(s)\,\big|_{s\to 1}\right)^2 = 1 + \frac{p_Z}{Z} \tag{6}$$

This looks relatively simple, but calculating p_Z is quite complicated and will therefore be performed in the appendix D. Here it shall be sufficient to note that $p_Z \to 1$ for $Z >> 1$, so in this case $g^{(2)} \approx 1$ and $p_Z \approx Z$ for $Z << 1$ and $g^{(2)} \approx 2$. For un-modulated thermal light the photon correlation is thus restricted to values between 1 and 2.

We also note here that the result above is independent of the temperature of the emitter. Still, for real experiments high temperatures are strongly favored, as one then has more photons per single measurement on average and a small enough statistical error is reached faster.

3 The key result: the second order correlation coefficient $g^{(2)}$

Motivated by a realistic star-like experimental configuration of a circular source and a rectangular detector geometry, we concentrate in the following on the $g^{(2)}$ function obtained in the appendix E for this geometry (Eq. E.3 and Eq. 8).

In addition and as also discussed in the appendix F, we have to consider partial coherence effects due to dark counts and the extended filter transmission curves of the Fabry–Perot interferometers by a factor β^2 in front of the four-fold Bessel integral which leads finally to the key result: the second order correlation coefficient $g^{(2)}$ for a circular source - rectangular detector geometry with integration variables r_1 and r_2 denoting points within the detector area S:

$$g^{(2)} = 1 + \frac{\beta^2}{S^2} \int_S \int_S \left|\frac{2J_1(\xi)}{\xi}\right|^2 d^2r_1 d^2r_2 \tag{7}$$

With x_i and y_i being the components of r_i, the argument of the Bessel function amounts to $\xi = \xi_0 \cdot r_{12} = \xi_0\sqrt{(x_2 - x_1)^2 + (y_2 - y_1)^2}$, where $\xi_0 = (k_0 \cdot d/2)/R = (2\pi \cdot d)/(2 \cdot \lambda \cdot R)$, with the source radius $d/2$ and the source-detector-distance R. The Papoulis simplification (see appendix E) reduces this to a double integral for a single vector (x, y) over the detector width and height dimensions Δx and Δy, and we finally obtain the key expression for $g^{(2)}$ for a circular source - rectangular detector geometry:

$$g^{(2)} = 1 + \frac{4\beta^2}{\Delta x^2 \Delta y^2} \times \int_0^{\Delta x} \int_0^{\Delta y} (\Delta x - x)(\Delta y - y) \left| \frac{2J_1\left(\xi_0 \sqrt{x^2 + y^2}\right)}{\xi_0 \sqrt{x^2 + y^2}} \right|^2 dxdy \quad (8)$$

4 Discussions of $g^{(2)}$

In the framework of the calculations we always consider "good" temporal coherence $Z_t << 1$ (see also section experimental set-up). According to Eq. D.1 and Eq. 8 the second order correlation coefficient $g^{(2)}$ depends on the spatial coherence parameter Z_s for good temporal coherence Z_t. $g^{(2)}$ thus depends on the source geometry and its dimensions, the detector geometry and its dimensions, and the distance between source and detector R. In the following, we concentrate on modelling these dependencies for a circular source geometry and a rectangular detector geometry and with parameters which will be also realized in the experimental section.

In order to compare and understand the $g^{(2)}$ results, we numerically integrate Eq. 8 for discrete parameter values and visualize the modelling results in terms of 3D-Plots and cuts through them. First, we depict graphically in Figs. 2 and 3 the results in terms of a corresponding 3D-Plot of $g^{(2)}$ as function of source diameter d and detector dimensions Δx and Δy (being here chosen equal for simplicity) for two source-detector distances R of 180 μm and 1000 μm. We then discuss the calculated results for $g^{(2)}$ in terms of cuts through these 3-D plots as shown in Figs. 2 and 3 in dependence on the characteristic parameters of $g^{(2)}$ and we explore what we can learn from the statistics regarding the properties of the emitting light source in terms of a real-world

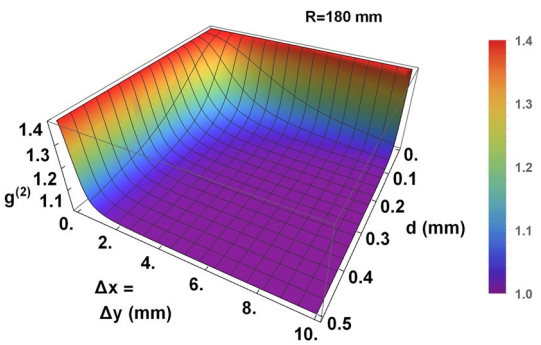

Fig. 2 3D-Plot of the second order correlation coefficient $g^{(2)}$ as a function of source diameter d and detector dimensions $\Delta x = \Delta y$ for a source-detector distance $R = 180$ mm

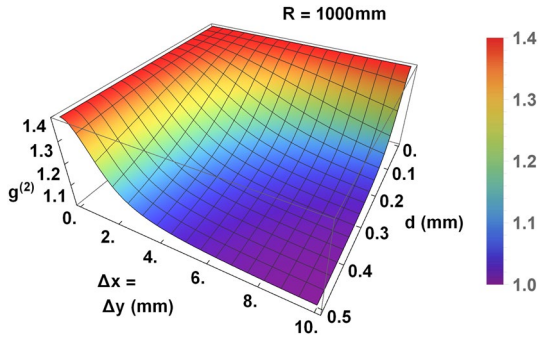

Fig. 3 3D-Plot of the second order correlation coefficient $g^{(2)}$ as a function of source diameter d and detector dimensions $\Delta x = \Delta y$ for a source-detector distance $R = 1000$ mm

application. Finally, at the end after the discussions of the modelling results, we show experimental results for four true thermal light source configurations and compare and discuss them with the developed model and derive a novel scheme in the spirit of the Hanbury Brown and Twiss experiment.

The general overall tendency of the modelling results as both found in the 3-D plots (Figs. 2, 3) and even more clearly visible in the cuts thereof, Figs. 4, 5, 6, and 7 can be best summarized as:

- The $g^{(2)}$ results as a function of the abscissa exhibit always the same kind of shape (in the 3-D plots) having the highest value of approximately $1 + \beta^2$ at an abscissa value of zero.
- With increasing abscissa values (d, Δx or Δy) $g^{(2)}$ is monotonously and asymptotically decreasing to a $g^{(2)}$ value of 1.0.
- With increasing d there is a decrease of $g^{(2)}$, and this decrease occurs faster for larger $\Delta x = \Delta y$ values.

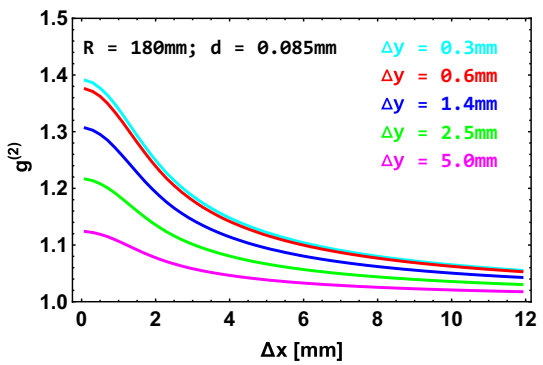

Fig. 4 Second order correlation coefficient $g^{(2)}$ as a function of rectangular detector width Δx for five rectangular detector heights Δy for a circular source diameter $d = 85$ μm and a source-detector distance $R = 180$ mm

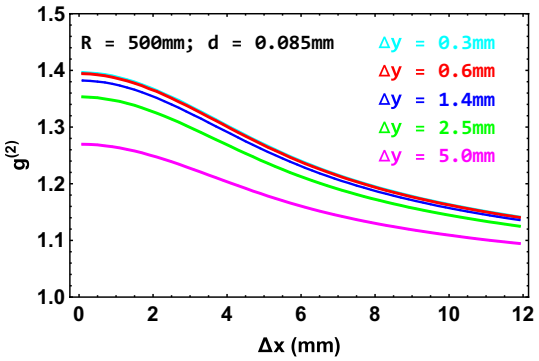

Fig. 5 Second order correlation coefficient $g^{(2)}$ as a function of rectangular detector width Δx for five rectangular detector heights Δy for a circular source diameter $d = 85$ μm and a source-detector distance $R = 500$ mm

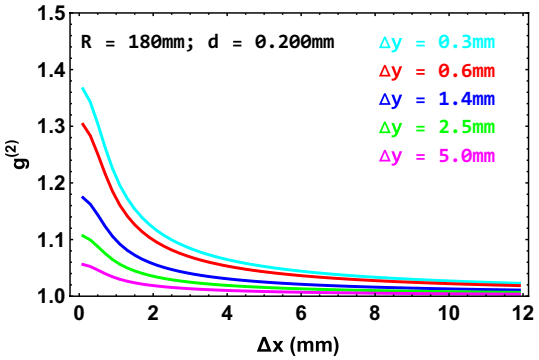

Fig. 6 Second order correlation coefficient $g^{(2)}$ as a function of rectangular detector width Δx for five rectangular detector heights Δy for a circular source diameter $d = 200$ μm and a source-detector distance $R = 180$ mm

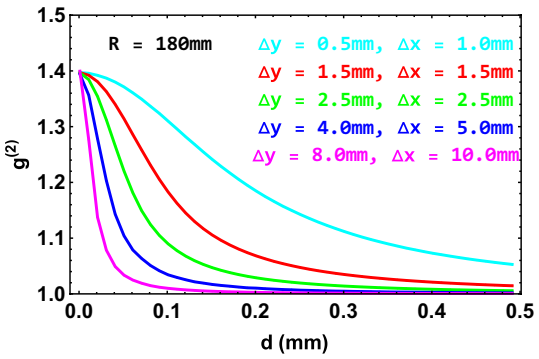

Fig. 7 Second order correlation coefficient $g^{(2)}$ as a function of circular source diameter d for five square detectors of dimensions $\Delta x = \Delta y$ for a source-detector distance $R = 180$ mm

- For larger detector source distances R this overall decrease of $g^{(2)}$ both in the d and $\Delta x = \Delta y$ direction occurs slower.

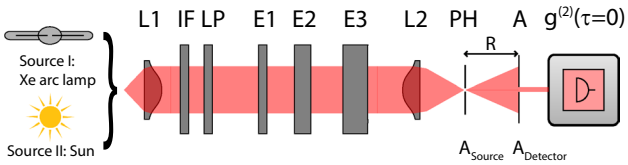

Fig. 8 Experimental set-up for the investigations of $g^{(2)}$ of the sun and the Xe arc lamp as a function of their spatial coherence; L lenses, IF interference filter, LP Linear Polarizer, E1, E2, and E3 Etalons, PH pin hole determining the effective source area A_{source} and at a distance R from it a second aperture A determining the effective detector area A_{detector} (c.f. Fig. 1), $g^{(2)}$ photon counting system for the determination of $g^{(2)}$ by a coincidence set-up

- This behaviour is also reflected by the cuts through the 3D plots as depicted in Figs. 4, 5, 6, and 7.
- The comparison between Fig. 4 and Fig. 6 shows that for larger source diameters d also the decay of $g^{(2)}$ with increasing Δx is faster.
- The maximum value of $g^{(2)}$ both for nearly zero Δx and d values decrease with increasing Δy.
- This decrease is slower for larger source - detector distance R and is faster for larger source diameter d.
- If we realize a quadratic detector ($\Delta x = \Delta y$) and investigate the $g^{(2)}$ behaviour as a function of the source diameter d the general behaviour is reproduced but becomes more and more steep with increasing $\Delta x = \Delta y$.

All these results, however most importantly the uniqueness of $g^{(2)}$ as a function of the spatial coherence parameter $Z_s = \frac{A_{\text{detector}} A_{\text{source}}}{\lambda^2 R^2}$, which is determined by the source properties and by the experimental setup allow now reversely to determine the spatial coherence parameter from a measurement of $g^{(2)}$. This opens a completely novel possibility for a method for the determination of an unknown parameter of the spatial coherence Z_s (i.e. e.g. source area or source-detector distance) when the other three parameters are known by measuring $g^{(2)}$. The essence of this here derived new HBT measurement scheme based on the fmgf and the $g^{(2)}$ function will subsequently be considered in the second part of the discussions after the depiction of the experimental set-up and the discussion of the experimental results.

5 Experimental set-up

Therefore, motivated by the modelling results for $g^{(2)}$ in dependence of the spatial coherence as depicted in Figs. 2, 3, 4, 5, 6, and 7, we have conceived and realized an experimental set-up (depicted in Fig. 8) to investigate this relation experimentally [65, 66].

As light source we have chosen two different thermal black-body sources, a Xe arc lamp and sun light. The light

emitted by both sources is collected and in the collimated beam we perform a highly selective spectral filtering in order to meet the requirement to have a sufficiently good temporal coherence corresponding to a small temporal coherence parameter $Z_t = \Delta\nu \cdot \Delta t$. A similar type of experimental configuration has been used by Kurtsiefer's group to comprehensively study temporal photon bunching of various terrestrial and astronomical sources [67, 68]. We used three etalons E_1, E_2 and E_3 in combination with an interference filter (IF) with free spectral range and spectral resolution data as depicted in Table 1. With our multiple Fabry–Perot filter or etalon configuration at a wavelength of 775 nm we realized a $\Delta\nu = 150$ MHz which together with the time resolution of the photon counting set-up of 1.05 ns results in a temporal coherence $Z_t = \Delta t \cdot \Delta\nu = 0.26$ [65].

The optical beam emitted by the different sources is then focused onto a pinhole (PH, diameter = 85 μm) which serves as the effective light source with an area $A_{\text{source}} = 5.67 \cdot 10^{-9}\text{m}^2$. The beam then incoherently illuminates an aperture (A) with variable width Δx and fixed height Δy which defines the effective detector area $A_{\text{detector}} = \Delta x \cdot \Delta y$. The distance R between these two apertures has been kept constant. In the case of the Xe arc lamp we used three different apertures with fixed height of $\Delta y = 0.6$ mm, 1.4 mm, and 2.5 mm yielding the data Xe06, Xe14, and Xe25, respectively. For the sun light investigations Δy amounts to 0.7 mm and R has been chosen to 0.195 m (data sun). Here, the light had been guided via a sun-tracker to the set-up.

The second order correlation coefficient $g^{(2)}$ could have been measured with a single photon-counting photomultiplier (PMT) with subsequently following counting electronics where mean and variance are derived from the photon counting probability distribution [69]. We have chosen a coincidence method instead by using a beam-splitter and two PMTs, thus reducing dead-time effects [70]. Typical count rates for the sun as light source to be investigated have been from 30.500 cps to approx. 80.000 cps, depending on the realized spatial coherence yielding in measurement times from 20 min up to 40 min and for the Xe lamp typical count rates have been from 40.000 cps to approx. 90.000 cps with measurement times between 40 min up to 14 h, respectively. The geometrical parameters of the experimental set-up represent all ingredients of the spatial coherence parameter $Z_s = \frac{A_{\text{detector}} A_{\text{source}}}{\lambda^2 R^2}$, entering the subsequently following modelling of the experimental $g^{(2)}$ values which both are jointly plotted in Figs. 9 and 10.

Table 1 Etalon and interference filter spectral characteristic data

Etalons and interference filters		
	Free spectral range (FSR)	Spectral resolution (FWHM)
Etalon no.1	1.5 THz (3.0 nm)	45.5. GHz (91pm)
Etalon no.2	75 GHz (150 pm)	2.3 GHz (4.6 pm)
Etalon no.3	5.0 GHz (10 pm)	155 MHz (0.31 pm)
Interference filter	@775 nm	763 GHz (1.5 nm)

6 Experimental results for $g^{(2)}$: discussion and comparison with modelling results

Figures 9 and 10 show the experimental results for $g^{(2)}$ as a function of the detector width Δx for fixed detector height Δy for the four true thermal light source configurations, 3 Xenon arc lamp results (Fig. 9) and one for the sun light (Fig. 10),

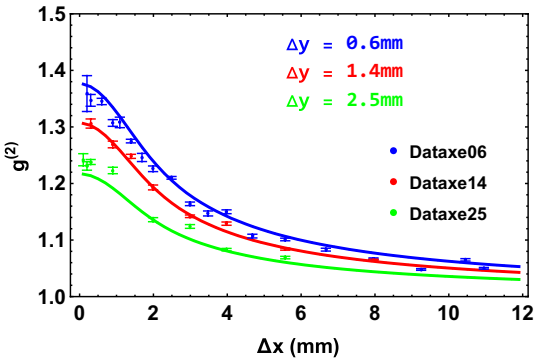

Fig. 9 Experimental results for $g^{(2)}$ measured as a function of the rectangular detector width δx for three detector heights $\delta y = 0.6$ mm (Datax06), 1.4 mm (Dataxe14), and 2.5 mm (Dataxe25) with a xenon arc lamp source together with modelling results according to Eq. 8 for $g^{(2)}$ considering a source diameter $d = 85$ μm and a source detector distance $R = 180$ mm (c.f. Fig. 8). Temporal coherence with $Z_t << 1$ has always been realized

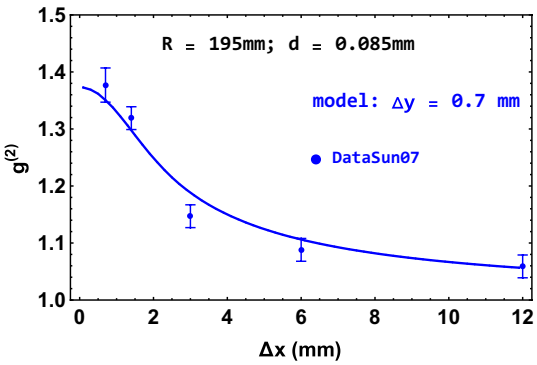

Fig. 10 Experimental results for $g^{(2)}$ measured as a function of the rectangular detector width Δx for a detector height Δy= 0.7 mm with the sun as source together with modelling results according to Eq. 8 for $g^{(2)}$ with the corresponding parameters. Temporal coherence with $Z_t << 1$ has been realized

respectively together with the model values already shown in Fig. 4. The experimental results clearly exhibit the S-shaped curve discussed above. Besides this qualitative agreement, we find excellent quantitative agreement with the modelling results if the real-world parameters for R, d, Δx and Δy are inserted. The coherence reduction factor β as discussed in subsection F of the appendix has been calculated to be $\beta = 0.63$ resulting in $\beta^2 = 0.397$. We find that with increasing Δx values the second order correlation coefficient $g^{(2)}$ is decreasing from approximately 1.4 towards an asymptotic value of 1.0 for Δx values beyond 12 mm.

We remind here as outlined before that the experimentally observed maximum value $g^{(2)}(0)$ is far from the theoretically expected value of $g^{(2)}(0)$ of 2.0 of ideal thermal sources and with ideal detection. We have to consider that in the experiment we do not only have the "coherent" light, but also a large number of spectrally distributed low intensity side lobes in the arrangement of the etalons as discussed in the appendix F. The light in these spectral side lobes sums up to quite a substantial incoherent contribution to the measurement, which effectively reduces $g^{(2)}$. With this modification as considered by the factor β, our the experimental data are in very good agreement with the theoretical $g^{(2)}$ values.

7 Renascence of Hanbury Brown and Twiss experiment towards star diameter determination

Finally, this first single-detector $g^{(2)}$ measurement of a true thermal light source as a function of the spatial coherence parameter together with the analytical expression for $g^{(2)}$ derived from the fmgf suggests a novel measurement technique for determining one of the ingredient parameters of Z_S, specifically the source area A_{source}, because usually the detector area A_{detector}, the wavelength λ and the distance R between source and detector are known. An hypothetical example for such a measurement procedure is illustrated by Fig. 11 and Table 2.

- Let us assume that we have an experimental configuration as listed in Table 2 with a wavelength $\lambda = 775$ nm, a detector source distance of $R = 180$ mm, and a detector height of $\Delta y = 1.0$ mm and a source diameter $d = 0.63$ mm, where the source diameter could not be measured directly in the experiment. Within our elaborated approach, we therefore perform a full hypothetical series of measurements of $g^{(2)}$ for 3 detector widths $\Delta x = 0.5$ mm, 1.5 mm, and 10.0 mm with the results as depicted in Table 2.

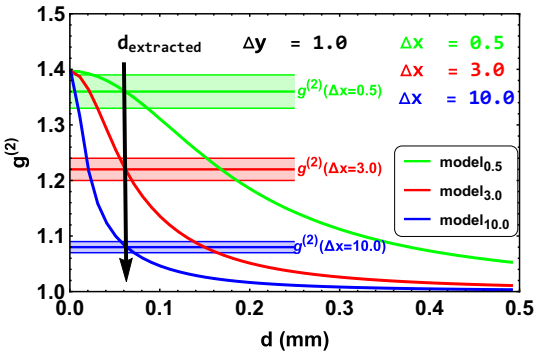

Fig. 11 Example experiment for the determination of an unknown source diameter: The experimental data of three $g^{(2)}$ measurements (including error bars) of an experimental situation as listed in Table 2 for three detector widths Δx are plotted in connection with modelling results according to (Eq. 8). The intersection between the $g^{(2)}$ values and the corresponding modelling results yields the source diameter d with the corresponding error bars

Table 2 Hypothetical measurement data for a source diameter determination

Detector height Δ y (mm)	1.0	1.0	1.0
Detector width Δ x (mm)	0.5	3.0	10.0
$g^{(2)}$ hypothetical experiment	$\left(1.36^{+0.3}_{-0.1}\right)$	$\left(1.22^{+0.2}_{-0.3}\right)$	$\left(1.08^{+0.1}_{-0.2}\right)$
Extracted source diameter d (mm)	$\left(0.06^{+0.02}_{-0.035}\right)$	$\left(0.063^{+0.07}_{-0.07}\right)$	$\left(0.063^{+0.07}_{-0.07}\right)$

- These experimental results for $g^{(2)}$ for the three detector widths Δx are then plotted in the framework of the modelling results for $g^{(2)}$ as horizontal line (with error bands) in Fig. 11 and the intersection point with the corresponding modelling curve is determined (including the error bars) for each detector width.
- The abscissa values of the intersection points yield the source diameter d. For the hypothetical sketched experiment, we obtain a value of $d = \left(0.063^{+0.07}_{-0.07}\right)$ demonstrating that in fact the source diameter can be extracted by this measurement idea and configuration.

Thus, this configuration idea based on the application of Eq. 8 represents a suggestion for a novel method for determining spatial coherence parameters, as e.g. the source dimensions in the spirit of a renascence of the HBT experiment. However, the limitations regarding the resolution of our scheme are equivalently challenging as the original HBT [71]. Moreover, our scheme represents a different approach and probably even today, and particularly stimulated by new activities in "quantum metrology" new metrology aspects,

either for very large or for very small thermal light emitter scales can be envisioned, i.e. "determining the size of a thermal emitter without measuring it directly" only by measuring the photon statistics of its emitted light alone with a single detector and analyzing the photon statistics.

8 Summary

We calculated the second order correlation coefficient $g^{(2)}$ of light emitted by a real-world thermal light source and absorbed by a photodetector resulting in click events using a factorial moment-generating function for the probability distribution. For good temporal coherence we find that $g^{(2)}$ reflects predominantly the spatial coherence function of the source, thus yielding an experimental technique to determine spatial coherence properties from single-detector $g^{(2)}$ measurements. The predicted dependencies have then been experimentally studied and discussed for three configurations of a thermal Xe arc light source and for the sun light as true thermal light sources. The good agreement between the experimental results for the four light source configurations and the calculated $g^{(2)}$ based on the factorial moment-generating function opens real-world perspectives for a novel type of HBT experiment allowing, e.g. to determine a light source diameter with a single-detector scheme. This progress gives fresh insight into the Hanbury Brown and Twiss experiment thus enabling a renascence even after 67 years.

9 Appendix

In these appendices we derive the second order correlation function $g^{(2)}$ based on a combination of a binomial detection process and a generalized Poisson statistics of the impinging radiation based on a Planck-Einstein approach for the photon partial systems and a classical probability approach for the a-priori probability, reflecting spatial and temporal coherence. Starting with a Poisson distribution, we develop the probability distribution of the detected photons in terms of a generalized Negative Binomial Distribution depending on the detected modes, their number and the a-priori detection probability. The a-priori-probability is then calculated for two selected geometries resulting in an expression for $g^{(2)}$ as function of detector area, source area, wavelength and distance between source and detector yielding finally an expression applicable on the experimental data. Finally, the influence of temporal incoherent light contributions will be considered.

A Partial sub-systems

The foundation of the thermodynamics of electromagnetic radiation is the quantized harmonic oscillator going back in its origins to Planck [72–74] where its energy E can be written as

$$E = \sum_{m=0}^{\infty} (m\hbar\omega)\omega_m = \hbar\omega \frac{\sum_{m=0}^{\infty} m e^{-m\gamma}}{\sum_{m=0}^{\infty} e^{-m\gamma}} = \hbar\omega \frac{1 \cdot e^{-\gamma} + 2 \cdot e^{-2\gamma} + 3 \cdot e^{-3\gamma} + \ldots}{1 + e^{-\gamma} + e^{-2\gamma} + e^{-3\gamma} + \ldots} = \hbar\omega \frac{1}{e^{\gamma} - 1}, \tag{A.1}$$

where $\gamma = \frac{\hbar\omega}{k_B T}$ with k_B being the Boltzmann constant. We note that this has the form of a geometric series, namely

$$E = \hbar\omega \frac{1}{e^{\gamma} - 1} = (\hbar\omega)(e^{-\gamma} + e^{-2\gamma} + e^{-3\gamma} + \ldots) = \hbar\omega \sum_{r=1}^{\infty} e^{-r\gamma} \tag{A.2}$$

where r=1, 2, 3,.. take here the role of quantum numbers. By Eq. (A.2) the system of the electromagnetic radiation is factorized into denumerably infinite many sub systems which are statistically independent. This allows computing the observed photon distribution from that of the individual r-subsystems [66], a big advantage in the statistical treatment of radiation. The factorial moment generating function of the observed photon distribution can be written as the product of the fmgfs of the single r-systems. The partial systems can be each regarded as an ideal gas as has been already done by Einstein [75].

B Statistics basics: Poisson distribution

One might expect that the photons in thermal radiation are independent from each other. In this case the repeated photon counting experiment as described in the main part of the manuscript would be described by a Poisson statistics

$$G_{\text{Poisson}}(s) = e^{M(s-1)}, \tag{B.1}$$

with the mean value $M = \langle m \rangle$ and the reduced autocorrelation $g^{(2)}$ would always be 1:

$$g^{(2)}_{Poisson}(s) = \frac{G''_{Poisson}(s=1)}{(G'_{Poisson}(s=1))^2} = \frac{\langle m \rangle^2}{\langle m \rangle^2} = 1, \tag{B.2}$$

Our measurements (and many others, see, e.g. [15, 16, 67, 68]) have shown, that this is not true, thermal radiation is more interesting than that and $g^{(2)}_{\text{thermal light}}$ is exceeding one.

C Towards Negative Binomial distribution

Instead, thermal light can be described using the independent sub-systems numbered here with an integer r denoting the number of photons within an "elementary bundle" or "radiation unit" of the radiation [76]. This elementary bundle replaces the all-too-simple concept of a light ray, taking the wave properties of the radiation into account. It is defined by the emitter properties, that is, its area and shape and its wavelength spectrum. According to the uncertainty principle, the direction of the energy transport is not defined precisely, but will instead be angularly spread out in inverse relation to the source dimension, roughly within $\Delta\Omega_{\text{diffraction}}$. Similarly, the timing of absorption events is again spread out in inverse relation to the width of the spectrum, roughly within $\Delta T_{\text{spectrum}}$. Both these effects are quantitatively described by the Fourier Transform of the respective source properties, which we shall exploit below performing the actual calculations for specifically selected special cases.

Here, we define a spatio-temporal "measurement volume" $V_{\text{measure}} = A_{\text{detector}} \cdot c \cdot \Delta t$ consisting out of the product of the detector area A_{detector} and the propagation length $c \cdot \Delta t$ within the measurement time. We also define a "coherence volume":

$$V_{\text{coh}} = S_{\text{coh}} \cdot l_{\text{coh}} = \frac{\lambda^2 R^2}{A_{\text{source}}} \cdot \frac{c}{\Delta\nu_{\text{spectrum}}} = \frac{\lambda^2 R^2 c \Delta T_{\text{spectrum}}}{A_{\text{source}}} \tag{C.1}$$

Dividing the measurement volume V_{measure} by this coherence volume V_{coh} yields the number of elementary bundles

$$N_{\text{elementary bundles}} = \frac{V_{\text{measure}}}{V_{\text{coh}}} = \frac{A_{\text{source}}}{\lambda^2 R^2 c \Delta T_{\text{spectrum}}} \cdot A_{\text{detector}} c \Delta t = \frac{A_{\text{source}} \cdot A_{\text{detector}} \cdot \Delta\nu_{\text{spectrum}} \cdot \Delta t}{\lambda^2 R^2} \tag{C.2}$$

Comparing this result to our definition of the coherence parameter Z according to Eq. (1) we find that the coherence parameter Z is just the number of elementary bundles $N_{\text{elementary bundles}}$ within our measurement.

We note that the measurement volume can have arbitrarily small or large values for both Δt and/or A_{Detector} which together with R^2 defines a solid angle as seen from the emitter $\Delta\Omega = A_{\text{Detector}}/R^2$. Values $Z < 1$ just mean, that the measurement is well inside the coherence length of the radiation, at least for one dimension.

We also remark, that this number of elementary bundles is also called number of phase cells of phase space, degrees of freedom of light, number of propagating modes or Jean's number [77, 78].

These elementary bundles or radiation units for propagating radiation are in some aspects comparable to the "oscillators" in the description of radiation in a cavity. Both can be "excited" to contain an integer number of energy packets, the photons, and the excited elementary bundle can be considered as non-interacting radiation units. They therefore obey a Poisson distribution.

For the probability distribution of the total radiation, the number N_r of the radiation units in a single r-system is proportional to $1/r$, and they follow a Poisson distributions with a unit number $N_r = \frac{Z}{rp_Z} e^{-r\gamma}$. With Eq. (B.1) we obtain for the factorial moment-generating function

$$G_{\text{r}}(s) = e^{\frac{Z}{rp_Z} exp(-r\gamma)(s-1)} \tag{C.3}$$

We are interested in the statistics of the photons and not in that of the radiation units which requires a re-scaling of the variables $k_{\text{radiation units}} \cdot r = k_{\text{photons}}$ and thus $G_{r,\text{photons}}(s) = \langle s^k_{\text{photon},r} \rangle = \langle s^{r \cdot k_{\text{radiation units}}} \rangle$. This transforms to

$$G_{\text{Photon}}(s) = \prod_{r=1}^{\infty} G_{r,\text{Photon}} = exp^{\sum_{r=1}^{\infty} \frac{Z}{rp_Z} e^{-r\gamma}(s^r - 1)} \tag{C.4}$$

and considering

$$\sum_{i=1}^{\infty} \frac{x^i}{i} = -ln(1-x) \tag{C.5}$$

we obtain

$$G_{\text{Photon}}(s) = \left(\frac{1 - se^{-\gamma}}{1 - e^{-\gamma}} \right)^{\frac{-Z}{p_Z}} = \left(1 - \frac{e^{-\gamma}}{1 - e^{-\gamma}} (s-1) \right)^{\frac{-Z}{p_Z}} = (1 - n_{Ph}(s-1))^{\frac{-Z}{p_Z}} \tag{C.6}$$

where in the last step the photon number per coherence volume has been inserted according to Eq. A.1:

$$n_{Ph} = \frac{e^{-\gamma}}{1 - e^{-\gamma}} \tag{C.7}$$

Finally, we observe that our detector - since it is potentially smaller than the "size" of the radiation units (calculation

below) - will only "see" an a-priori-fraction p_Z with its quantum efficiency of η and so it will only register this fraction of photons and we obtain for the by clicks registered photons

$$G_{\text{clicks}}(s) = (1 - \eta n_{Ph} p_Z (s-1))^{\frac{-Z}{p_Z}} \tag{C.8}$$

For the mean value of the clicks we correctly obtain:

$$\langle m \rangle = \frac{d}{ds} G_{\text{clicks}}(s) \mid_{s\to 1} = \eta n_{Ph} Z \tag{C.9}$$

From the expression of the factorial moments, derived in the general case from G(s) or in our case from the photodetected clicks $G_{\text{clicks}}(s)$ (Eq. C.8) the probability distribution $w(k)$ is obtained according to Ref. [5, 27]:

$$\begin{aligned} w(k) &= \frac{1}{k!}\frac{d^k}{ds^k} G_{\text{clicks}}(s) \mid_{s\to 0} \\ &= \frac{\Gamma\left(\frac{Z}{p_Z} + k\right)}{\Gamma\left(\frac{Z}{p_Z}\right)\Gamma(k+1)} \frac{(\eta n_{Ph} p_Z)^k}{(1 + \eta n_{Ph} p_Z)^{\frac{Z}{p_Z}+k}} = w_{\text{NBD}}(k) \end{aligned} \tag{C.10}$$

which is the well-known Negative Binomial or Polya Distribution [27] with the second order correlation coefficient

$$g^{(2)} = \frac{\frac{d^2}{ds^2} G_{\text{clicks}}(s) \mid s=1}{\left(\frac{d}{ds} G_{\text{clicks}}(s) \mid s=1\right)^2} = 1 + \frac{p_Z}{Z}. \tag{C.11}$$

D Calculation of p_Z

To calculate the effective a-priori-probability p_Z we again observe that the radiation units or elementary bundles are extended in space, shaped by the properties of the light source due to the uncertainty principle. They may travel in any direction: with their center of gravity right towards the center of the detector, off-center, towards the detector edge, or even outside the detector. We use a coordinate pair (u, v) within the detector plane to designate this direction from the light source, meaning the center of gravity of a radiation unit while hitting the detector would be at (u, v).

The photons of this radiation unit may then be found scattered around this spot. A specific photon may appear at position (u', v') with the normalized probability density $q(u' - u, v' - v)$. This is the absolute square of the Fourier transform of the light source shape $S(x, y)$, normalized to $\int_{\Delta Z} q(u' - u, v' - v) du' dv' = 1$. This can be understood in some sense as reminescence of the Van Zittert-Zernike theorem [27, 79–81]. In case of a rectangular light source with $A_{\text{source}} = x_{\text{source}} \cdot y_{\text{source}} = 2h \cdot 2w$ the Fourier transform separates into x and y components, and each are sinc-functions. In case of a circular light source the shape of q is the well-known Airy-disk. In the general case, the 2-dimensional Fourier transform has to be calculated numerically.

The a-priori-probability p_Z can now be calculated by integrating the probability density of photons that fall into the detector sensitive area Z:

$$p_Z = \frac{1}{Z} \int_Z \int_Z q(u' - u, v' - v) du du' dv dv' \tag{D.1}$$

The factor $\frac{1}{Z}$ ensures that for $Z_x >> 1$ and $Z_y >> 1$ (very large detector) we get the normalization $p_Z \approx 1$. It follows that in the case $Z_x << 1$ and $Z_y << 1$ we get $p_Z \approx Z$. By inserting Eq. D.1 into C.11 we can calculate the desired $g^{(2)}$ from the parameters of the experimental setup.

E. Calculation of $g^{(2)}$ for selected geometries

1. For a rectangular source (dimensions height $2h$ and width $2w$) and rectangular detector (dimensions Δ x and Δ y) Eqs. C.11 with D.1 yield:

$$\begin{aligned} g^{(2)} = 1 + \frac{1}{(\Delta x \Delta y)^2} \times \\ \int_{-\Delta x/2}^{\Delta x/2} \int_{-\Delta x/2}^{\Delta x/2} \int_{-\Delta y/2}^{\Delta y/2} \int_{-\Delta y/2}^{\Delta y/2} \\ \left| \frac{sin\frac{k_o h}{R}(x_1 - x_2)}{\frac{k_o h}{R}(x_1 - x_2)} \frac{sin\frac{k_o w}{R}(y_1 - y_2)}{\frac{k_o w}{R}(y_1 - y_2)} \right|^2 dx_1 dx_2 dy_1 dy_2 \end{aligned} \tag{E.1}$$

where

$$|\mu(r_1, r_2)| = \left| \frac{sin\frac{k_o h}{R}(x_1 - x_2)}{\frac{k_o h}{R}(x_1 - x_2)} \frac{sin\frac{k_o w}{R}(y_1 - y_2)}{\frac{k_o w}{R}(y_1 - y_2)} \right| \tag{E.2}$$

can be recognized as the module of the normalized degree of coherence (for the case $D >> \rho$) between two points P_1 and P_2 in a plane (observation plane of r_1 and r_2) located at a distance R of an incoherent monochromatic rectangular source with the dimensions height $2h$ and width $2w$ and with wavelength λ and uniform brilliance [26].

2. For a circular source (diameter d or radius ρ) of uniform brilliance and a rectangular detector with surface S at a distance R we obtain

$$g^{(2)} = 1 + \frac{1}{S^2} \int_S \int_S \left| \frac{2J_1(k_0 \frac{\rho}{R} r_{12})}{(k_0 \frac{\rho}{R} r_{12})} \right|^2 dx_1 dx_2 dy_1 dy_2 \tag{E.3}$$

with $r_{12} = \sqrt{(x_2 - x_1)^2 + (y_2 - y_1)^2}$, the distance R between source and detector, and wavelength λ. Also here, the function under the integral

$$|\mu(r_1, r_2)| = \left| \frac{2J_1(k_0 \frac{\rho}{R} r_{12})}{(k_0 \frac{\rho}{R} r_{12})} \right| \tag{E.4}$$

can be recognized as the module of the normalized degree of coherence (for the case $R >> \rho$) between two points P_1 and P_2 in the observation plane. We define $\xi_0 = (k_0 \cdot d/2)/R = (2\pi \cdot d)/(2 \cdot \lambda \cdot R)$ and get

$$g^{(2)} = 1 + \frac{1}{(\Delta x \Delta y)^2} \times \int_{-\Delta x/2}^{\Delta x/2} \int_{-\Delta x/2}^{\Delta x/2} \int_{-\Delta y/2}^{\Delta y/2} \int_{-\Delta y/2}^{\Delta y/2} \left[\frac{2J_1\left(\xi_0 \sqrt{(x_2 - x_1)^2 + (y_2 - y_1)^2}\right)}{\xi_0 \sqrt{(x_2 - x_1)^2 + (y_2 - y_1)^2}} \right]^2 dx_1 dx_2 dy_1 dy_2 \tag{E.5}$$

The Papoulis Ansatz [82] according to

$$\int_{-L}^{L} \int_{-L}^{L} f(x_1 - x_2) dx_1 dx_2 = 2 \int_0^{2L} (2L - x) f(x) dx \tag{E.6}$$

allows finally a reduction of the fourfold integral (Eq. E.5) to a double integral

$$g^{(2)} = 1 + \frac{4}{(\Delta x \Delta y)^2} \int_0^{\Delta x} \int_0^{\Delta y} (\Delta x - x)(\Delta y - y) \left[\frac{2J_1\left(\xi_0 \sqrt{x^2 + y^2}\right)}{\xi_0 \sqrt{x^2 + y^2}} \right]^2 dx dy \tag{E.7}$$

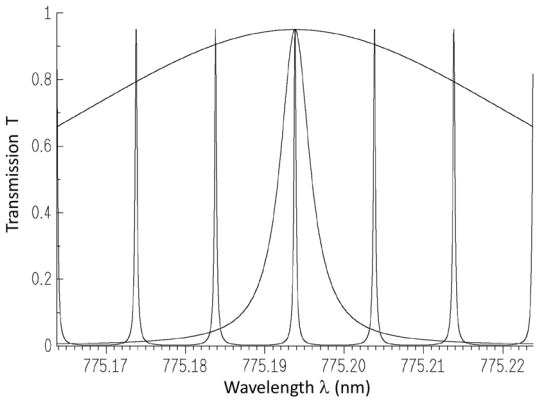

Fig. 12 Transmission of the etalons E1, E2, and E3. (See Fig. 8 and Table 1)

which is the basis of the calculations and discussions in the main part.

F The effect of incoherent light contributions

In principle the temporal coherence Z_t could be discussed the same way as the spatial coherence above. However, in our measurement setup (see section 5 Experimental set-up) the spectral distribution of the light is quite complex as it is realized by a combination of an interference filter and three different Etalons. We carefully matched the central wavelengths of the Etalons to the same values to get a very narrow $\Delta\nu$ central line, which together with the temporal resolution of our detector corresponds to a temporal coherence parameter $Z_t = 0.26$. We consider this to be sufficiently small so that $p_t \approx Z_t$.

However, it was unavoidable that a lot of further transmission peaks were also transmitted by the filter combination at small transmission ratios. Fig. 12 shows the theoretical transmission curves of the three etalons separately. In total we get the product of all three curves multiplied again by the transmission of the interference filter.

With this we have about $\beta = 62\%$ of the transmitted intensity in the central peak, while the residual light is distributed over a wide spectral range. For simplicity, we consider this residual light as an incoherent background intensity, which due to the wide spectral range (large Z_t) for itself exhibits a $g^{(2)}_{\text{background}} = 1$. In addition, photons from this background are also not correlated with the photons from the central peak, which reduces the measured $g^{(2)}$ further. A comprehensive treatment yields:

$$g^{(2)}_{\text{effective}} = 1 + \beta^2 \cdot (g^{(2)}_{\text{ideal thermal source}} - 1) \tag{F.1}$$

Therefore, for our realized experimental conditions we expect the value of $g^{(2)}$ in the limit $Z_x, Z_y \to 0$ to be around $1 + \beta^2 \approx 1.38$. The largest measured value is still a little bit smaller due to the finite Z_x and Z_y. However, this agrees very well with our actual measurement and modelling results shown in Fig. 9 and Fig. 10.

Acknowledgements This work was supported by Deutsche Forschungsgemeinschaft (DFG) (project EL 105-21). We would like to thank Peter Würfel for fruitful and stimulating discussions and valuable helpful support. One of the authors (WE) is particularly grateful to Andreas Herdt, Markus Rosskopf and Florian Kroh for support regarding MATHEMATICA and LATEX and to Herbert Egger for discussions on integration of Bessel functions.

Author contributions All authors contributed to the manuscript. The basic idea of radiation thermodynamics related to the Hanbury Brown and Twiss experiment originates from WR. The experiments have been realized and performed by JR in collaboration with PD. PD developed the mathematical treatment of the fluctuations of light. Both, JR and PD have been inspired and supervised by WR. The manuscript and its

first draft have been conceived by WE including the realization of the figures and sketching the hypothetical HBT renascence experiment.

Funding Open Access funding enabled and organized by Projekt DEAL.

Declarations

Conflict of interest The authors declare no competing interests.

References

1. R.J. Glauber, The quantum theory of optical coherence. Phys. Rev. **130**, 2529–2539 (1963). https://doi.org/10.1103/PhysRev.130.2529
2. E.R. Pike, Lasers, photon statistics, photon-correlation spectroscopy and subsequent applications. J. Eur. Opt. Soc. Rapid Publ. **5**, 10047 (2010). https://doi.org/10.2971/jeos.2010.10047s
3. R. Baltz, Photons and photon statistics: From incandescent light to lasers. Front. Opt. Spectr. NATO Sci. Ser. II Math. Phys. Chem. **168**, 55–92 (2005). https://doi.org/10.1007/1-4020-2751-6-3
4. L. Mandel, Fluctuations of photon beams: the distribution of the photo-electrons. Proceed. Phys. Soc. **74**(3), 233–243 (1959). https://doi.org/10.1088/0370-1328/74/3/301
5. B.E.A. Saleh, Photoelectron Statistics. Springer, Berlin, Heidelberg (1978). https://doi.org/10.1007/978-3-540-37311-7
6. R.H. Brown, R.Q. Twiss, Correlation between photons in two coherent beams of light. Nature **177**, 27–29 (1956). https://doi.org/10.1038/177027a0
7. V. Degiorgio, About photon correlations. Am. J. Phys. **81**(10), 772–775 (2013). https://doi.org/10.1119/1.4819319
8. R.J. Glauber, Photon correlations. Phys. Rev. Lett. **10**(3), 84–86 (1963). https://doi.org/10.1103/physrevlett.10.84
9. R.J. Glauber, Nobel lecture: one hundred years of light quanta. Rev. Mod. Phys. **78**(4), 1267–1278 (2006). https://doi.org/10.1103/revmodphys.78.1267
10. R.H. Brown, R.Q. Twiss, A test of a new type of stellar interferometer on sirius. Nature **178**(4541), 1046–1048 (1956). https://doi.org/10.1038/1781046a0
11. R.H. Brown, J. Davis, L.R. Allen, The angular diameters of 32 stars. Mon. Not. R. Astron. Soc. **167**(1), 121–136 (1974). https://doi.org/10.1093/mnras/167.1.121
12. P.K. Tan, G.H. Yeo, H.S. Poh, A.H. Chan, C. Kurtsiefer, Measuring temporal photon bunching in blackbody radiation. Astrophys. J. **789**(1), 10 (2014). https://doi.org/10.1088/2041-8205/789/1/l10
13. P.K. Tan, C. Kurtsiefer, Temporal intensity interferometry for characterization of very narrow spectral lines. Mon. Not. R. Astron. Soc. **469**(2), 1617–1621 (2017). https://doi.org/10.1093/mnras/stx968
14. C. Foellmi, Intensity interferometry and the second-order correlation function $g^{(2)}$ in astrophysics. Astronomy & Astrophysics **507**(3), 1719–1727 (2009). https://doi.org/10.1051/0004-6361/200911739
15. W. Guerin, A. Dussaux, M. Fouché, G. Labeyrie, J.-P. Rivet, D. Vernet, F. Vakili, R. Kaiser, Temporal intensity interferometry: photon bunching in three bright stars. Mon. Not. R. Astron. Soc. **472**(4), 4126–4132 (2017). https://doi.org/10.1093/mnras/stx2143
16. W. Guerin, J.-P. Rivet, M. Fouché, G. Labeyrie, D. Vernet, F. Vakili, R. Kaiser, Spatial intensity interferometry on three bright stars. Mon. Not. R. Astron. Soc. **480**(1), 245–250 (2018). https://doi.org/10.1093/mnras/sty1792
17. S. LeBohec, C. Barbieri, W.-J. Wit, D. Dravins, P. Feautrier, C. Foellmi, A. Glindemann, J. Hall, J. Holder, R. Holmes, P. Kervella, D. Kieda, E.L. Coarer, S. Lipson, F. Malbet, S. Morel, P. Nuñez, A. Ofir, E. Ribak, S. Saha, M. Schoeller, B. Zhilyaev, H. Zinnecker, Toward a revival of stellar intensity interferometry. Proc. SPIE **7013**, 70132 (2008). https://doi.org/10.1117/12.787443
18. M. Drechsler, F. Lohof, C. Gies, Revisiting the siegert relation for the partially coherent regime of nanolasers. Appl. Phys. Lett. **120**(22), 221104 (2022). https://doi.org/10.1063/5.0094698
19. D. Ferreira, R. Bachelard, W. Guerin, R. Kaiser, M. Fouché, Connecting field and intensity correlations: The siegert relation and how to test it. Am. J. Phys. **88**(10), 831–837 (2020). https://doi.org/10.1119/10.0001630
20. F.T. Arecchi, E. Gatti, A. Sona, Time distribution of photons from coherent and gaussian sources. Phys. Lett. **20**(1), 27–29 (1966). https://doi.org/10.1016/0031-9163(66)91034-1
21. W. Martienssen, E. Spiller, Coherence and fluctuations in light beams. Am. J. Phys. **32**(12), 919–926 (1964). https://doi.org/10.1119/1.1970023
22. W. Martienssen, E. Spiller, Intensity fluctuations in light beams with several degrees of freedom. Phys. Rev. Lett. **16**(12), 531–533 (1966). https://doi.org/10.1103/physrevlett.16.531
23. C.D. Cantrell, J.R. Fields, Effect of spatial coherence on the photoelectric counting statistics of gaussian light. Phys. Rev. A **7**(6), 2063–2069 (1973). https://doi.org/10.1103/physreva.7.2063
24. J. Bures, C. Delisle, A. Zardecki, Détermination de la surface de cohérence à partir d'une expérience de photocomptage. Can. J. Phys. **50**(8), 760–768 (1972). https://doi.org/10.1139/p72-108
25. C. Delisle, J. Bures, Nouvelle méthode de mesure de la cohérence spatiale en lumière pseudo-thermique par comptage des photoélectrons. Can. J. Phys. **49**(14), 1940–1949 (1971). https://doi.org/10.1139/p71-233
26. M. Born, E. Wolf, *Principles of optics: electromagnetic theory of propagation, interference and diffraction of light, 2nd*, enlarged. (Cambridge University Press, Cambridge New York, 1999)
27. J.W. Goodman, *Statistical optics*, 2nd edn. (John Wiley & Sons Inc, Hoboken, New Jersey, 2015)
28. D. Scarl, Measurements of photon correlations in partially coherent light. Phys. Rev. **175**(5), 1661–1668 (1968). https://doi.org/10.1103/physrev.175.1661
29. D.F. Walls, Evidence for the quantum nature of light. Nature **280**, 451–454 (1979). https://doi.org/10.1038/280451a0
30. G. Lachs, Theoretical aspects of mixtures of thermal and coherent radiation. Phys. Rev. **138**(4B), 1012–1016 (1965). https://doi.org/10.1103/physrev.138.b1012
31. F.T. Arecchi, Measurement of the statistical distribution of gaussian and laser sources. Phys. Rev. Lett. **15**, 912 (1965). https://doi.org/10.1103/PhysRevLett.15.912
32. B.L. Morgan, L. Mandel, Measurement of photon bunching in a thermal light beam. Phys. Rev. Lett. **16**(22), 1012–1015 (1966). https://doi.org/10.1103/physrevlett.16.1012

33. T. Hassinen, J. Tervo, T. Setälä, A.T. Friberg, Hanbury brown–twiss effect with electromagnetic waves. Opt. Express **19**(16), 15188 (2011). https://doi.org/10.1364/oe.19.015188
34. T.J. Bartley, G. Donati, X.-M. Jin, A. Datta, M. Barbieri, I.A. Walmsley, Direct observation of sub-binomial light. Phys. Rev. Lett. **110**(17), 173602 (2013). https://doi.org/10.1103/physrevlett.110.173602
35. W.E. Hayenga, H. Garcia-Gracia, H. Hodaei, C. Reimer, R. Morandotti, P. LiKamWa, M. Khajavikhan, Second-order coherence properties of metallic nanolasers. Optica **3**(11), 1187 (2016). https://doi.org/10.1364/optica.3.001187
36. M. Marconi, J. Javaloyes, P. Hamel, F. Raineri, A. Levenson, A.M. Yacomotti, Far-from-equilibrium route to superthermal light in bimodal nanolasers. Phys. Rev. X **8**(1), 011013 (2018). https://doi.org/10.1103/physrevx.8.011013
37. M. Henny, S. Oberholzer, C. Strunk, T. Heinzel, K. Ensslin, M. Holland, C. Schönenberger, The fermionic hanbury brown and twiss experiment. Science **284**(5412), 296–298 (1999). https://doi.org/10.1126/science.284.5412.296
38. A.M.D. Mendoza, F. Caycedo-Soler, P. Manrique, L. Quiroga, F.J. Rodriguez, N.F. Johnson, Exploiting non-trivial spatio-temporal correlations of thermal radiation for sunlight harvesting. J. Phys. B: At. Mol. Opt. Phys. **50**(12), 124002 (2017). https://doi.org/10.1088/1361-6455/aa6e11
39. A.M.D. Mendoza, F. Caycedo-Soler, S.F. Huelga, M.B. Plenio, Temporal correlations of sunlight may assist photoprotection in bacterial photosynthesis. New J. Phys. **22**(7), 073042 (2020). https://doi.org/10.1088/1367-2630/ab99e0
40. P.D. Manrique, F. Caycedo-Soler, A.D. Mendoza, F. Rodríguez, L. Quiroga, N.F. Johnson, Exploring the effects of photon correlations from thermal sources on bacterial photosynthesis. Results Phys. **6**, 957–960 (2016). https://doi.org/10.1016/j.rinp.2016.11.024
41. M. Bertolotti, B. Crosignani, P. Porto, On the statistics of gaussian light scattered by a gaussian medium. J. Phys. A: Gen. Phys. **3**(5), 37–38 (1970). https://doi.org/10.1088/0305-4470/3/5/016
42. D. Newman, K distributions from doubly scattered light. J. Opt. Soc. Am. A **2**, 22–26 (1985). https://doi.org/10.1364/JOSAA.2.000022
43. K.A. O'Donnell, Speckle statistics of doubly scattered light. J. Opt. Soc. Am. **72**, 1459–1463 (1982). https://doi.org/10.1364/JOSAA.9.000091
44. M. Bondani, A. Allevi, Direct detection of super-thermal photon-number statistics in second harmonic generation. Opt. Lett. **40**, 3089–3092 (2015). https://doi.org/10.1364/OL.40.003089
45. A. Allevi, S. Cassina, M. Bondani, Super-thermal light for imaging applications. Quantum Meas. Quantum Metrol. **4**, 26–34 (2017). https://doi.org/10.1515/qmetro-2017-0004
46. F. Boitier, A. Godard, N. Dubreuil, P. Delaye, C. Fabre, E. Rosencher, Photon extrabunching in ultrabright twin beams measured by two-photon counting in a semiconductor. Nat. Commun. **2**, 425 (2011). https://doi.org/10.1038/ncomms1423
47. F. Boitier, A. Godard, E. Rosencher, C. Fabre, Measuring photon bunching at ultrashort timescale by two-photon-absorption in semiconductors. Nat. Phys. **5**, 267–270 (2009). https://doi.org/10.1038/nphys1218
48. V. Degiorgio, Photon bunching in chaotic fields with uni-dimensional probability density. Europhys. Lett. **98**, 44007 (2012). https://doi.org/10.1209/0295-5075/98/44007
49. G. Chesi, L. Malinverno, A. Allevi, R. Santoro, M. Caccia, A. Martemiyanov, M. Bondani, Optimizing silicon photomultipliers for quantum optics. Sci. Rep. **9**(1), 7433 (2019). https://doi.org/10.1038/s41598-019-43742-1
50. M. Bondani, A. Allevi, A. Andreoni, Light statistics by non-calibrated linear photodetectors. Adv. Sci. Lett. **2**(4), 463–468 (2009). https://doi.org/10.1166/asl.2009.1052
51. M.D. Eisaman, J. Fan, A. Migdall, S.V. Polyakov, Invited review article: Single-photon sources and detectors. Rev. Sci. Instrum. **82**(7), 071101 (2011). https://doi.org/10.1063/1.3610677
52. G. Zambra, A. Andreoni, M. Bondani, M. Gramegna, M. Genovese, G. Brida, A. Rossi, M.G.A. Paris, Experimental reconstruction of photon statistics without photon counting. Phys. Rev. Lett. **95**(6), 063602 (2005). https://doi.org/10.1103/physrevlett.95.063602
53. M. Bohmann, R. Kruse, J. Sperling, C. Silberhorn, W. Vogel, Direct calibration of click-counting detectors. Phys. Rev. A **95**(3), 033806 (2017). https://doi.org/10.1103/physreva.95.033806
54. R. Heilmann, J. Sperling, A. Perez-Leija, M. Gräfe, M. Heinrich, S. Nolte, W. Vogel, A. Szameit, Harnessing click detectors for the genuine characterization of light states. Sci. Rep. **6**(1), 19489 (2016). https://doi.org/10.1038/srep19489
55. J. Hloušek, M. Dudka, I. Straka, M. Ježek, Accurate detection of arbitrary photon statistics. Phys. Rev. Lett. **123**(15), 153604 (2019). https://doi.org/10.1103/physrevlett.123.153604
56. J.H. Shapiro, R.W. Boyd, The physics of ghost imaging. Quantum Inf. Process. **11**(4), 949–993 (2012). https://doi.org/10.1007/s11128-011-0356-5
57. M.J. Padgett, R.W. Boyd, An introduction to ghost imaging: quantum and classical. Philos. Trans. R. Soc. Lond A Math. Phys. Eng. Sci. **375**(2099), 20160233 (2017). https://doi.org/10.1098/rsta.2016.0233
58. B.I. Erkmen, J.H. Shapiro, Ghost imaging: from quantum to classical to computational. Adv. Opt. Photon. **2**(4), 405–450 (2010). https://doi.org/10.1364/AOP.2.000405
59. M. Genovese, Real applications of quantum imaging. J. Opt. **18**, 073002 (2016). https://doi.org/10.1088/2040-8978/18/7/073002
60. S. Hartmann, W. Elsäßer, A novel semiconductor-based, fully incoherent amplified spontaneous emission light source for ghost imaging. Sci. Rep. **7**, 41866 (2017). https://doi.org/10.1038/srep41866
61. B.J. Hoenders, Review of a bewildering classical-quantum phenomenon: ghost imaging. Adv. Imaging Electron Phys. **208**, pp. 1–44 (2018). https://doi.org/10.1016/bs.aiep.2018.08.001
62. P. Janassek, S. Blumenstein, W. Elsäßer, Ghost spectroscopy with classical thermal light emitted by a superluminescent diode. Phys. Rev. Appl. **9**, 021001 (2018). https://doi.org/10.1103/PhysRevApplied.9.021001
63. L.A. Lugiato, Ghost imaging: fundamental and applicative aspects. Istit Lomb (Rend Scienze) **147**, 139–148 (2013). https://doi.org/10.4081/scie.2013.169
64. R. Loudon, *The quantum theory of light* (Oxford University Press, Oxford, 2000)
65. J. Ross, Die Experimentelle Bestimmung Von Photonenkorrelationen in Thermischer Strahlung, Ph. D. Thesis, Universitaet Karlsruhe. Shaker, Aachen (1996)
66. P. Dürr, Die Bedeutung Von Raum und Zeit Bei der Thermodynamischen Behandlung der Fluktuationen Thermischer Strahlung, Ph. D. Thesis, Universität Karlsruhe. Shaker, Aachen (1995)
67. P.K. Tan, G.H. Yeo, H.S. Poh, A.H. Chan, C. Kurtsiefer, Measuring temporal photon bunching in blackbody radiation. Astrophys. J. **789**(1), 10 (2014). https://doi.org/10.1088/2041-8205/789/1/l10
68. P.K. Tan, C. Kurtsiefer, Temporal intensity interferometry for characterization of very narrow spectral lines. Mon. Not. R.

Astron. Soc. **469**(2), 1617–1621 (2017). https://doi.org/10.1093/mnras/stx968
69. S. Kuhn, S. Hartmann, W. Elsäßer, Photon-statistics-based classical ghost imaging with one single detector. Opt. Lett. **41**, 2863–2866 (2016). https://doi.org/10.1364/OL.41.002863
70. M. Beck, Comparing measurements of $g^{(}2)(0)$ performed with different coincidence detection techniques. J. Opt. Soc. Am. B **24**(12), 2972 (2007). https://doi.org/10.1364/josab.24.002972
71. R.H. Brown, The Intensity Interferometer - Its Application to Astronomy. Taylor & Francis, London (1974). Chap. 8
72. T.H. Boyer, Thermodynamics of the harmonic oscillator: derivation of the planck blackbody spectrum from pure thermodynamics. Eur. J. Phys. **40**(2), 025101 (2019). https://doi.org/10.1088/1361-6404/aaf45b
73. D. Kondepudi, I. Prigogine, Thermodynamics of radiation. In: Modern Thermodynamics, pp. 287–303. John Wiley & Sons, Chichester (2014). https://doi.org/10.1002/9781118698723.ch11
74. M. Planck, Ueber das gesetz der energieverteilung im normalspectrum. Ann. Phys. **309**(3), 553–563 (1901). https://doi.org/10.1002/andp.19013090310
75. M.J. Klein, Max planck and the beginnings of the quantum theory. Arch. Hist. Exact Sci. **1**(5), 459–479 (1962). https://doi.org/10.1007/BF00327765
76. M. Laue, Die freiheitsgrade von strahlenbündeln. Ann. Phys. **349**(16), 1197–1212 (1914). https://doi.org/10.1002/andp.19143491606
77. E. Wolf, *Introduction to the theory of coherence and polarization of light* (Cambridge University Press, Cambridge, 2007)
78. S. Varró, The role of self-coherence in correlations of bosons and fermions in linear counting experiments notes on the wave-particle duality. Fortschr. Phys. **59**(3–4), 296–324 (2010). https://doi.org/10.1002/prop.201000071
79. L. Mandel, E. Wolf, Coherence properties of optical fields. Rev. Mod. Phys. **37**(2), 231–287 (1965). https://doi.org/10.1103/revmodphys.37.231
80. F. Zernike, The concept of degree of coherence and its application to optical problems. Physica **5**(8), 785–795 (1938). https://doi.org/10.1016/s0031-8914(38)80203-2
81. P.H. Cittert, Die wahrscheinliche schwingungsverteilung in einer von einer lichtquelle direkt oder mittels einer linse beleuchteten ebene. Physica **1**(1–6), 201–210 (1934). https://doi.org/10.1016/s0031-8914(34)90026-4
82. A. Papoulis, S.U. Pillai, *Probability, Random Variables, and Stochastic Processes*, 4th edn. (McGraw-Hill, Boston, 2002), p.397